Development of CMOS dosimetry in proton minibeams for enhanced QA and primary standard absorbed dose calorimetry

Flynn, Samuel; Allport, Philip; De Marzi, Ludovic; Green, Stuart; Homer, Michael; Lee, Nigel; Ortiz, Ramon; Patriarca, Annalisa; Prezado, Yolanda; Thomas, Russell; Price, Tony

DOI:
10.1088/1748-0221/18/03/P03014

Development of CMOS dosimetry in proton minibeams for enhanced QA and primary standard absorbed dose calorimetry

Jinst

Published by IOP Publishing for Sissa Medialab

Received: November 7, 2022
Revised: January 13, 2023
Accepted: February 2, 2023
Published: March 9, 2023

Development of CMOS dosimetry in proton minibeams for enhanced QA and primary standard absorbed dose calorimetry

Samuel Flynn,[a,b,*] **Philip Allport,**[b] **Ludovic De Marzi,**[c] **Stuart Green,**[d] **Michael Homer,**[a] **Nigel Lee,**[a] **Ramon Ortiz,**[c,e] **Annalisa Patriarca,**[c] **Yolanda Prezado,**[c,e] **Russell Thomas**[a,f] **and Tony Price**[b,a]

[a] *Medical Radiation Science Group, National Physical Laboratory, Hampton Road, Teddington, TW11 0LW, United Kingdom*
[b] *School of Physics and Astronomy, University of Birmingham, Edgbaston Campus, Birmingham, B15 2TT, United Kingdom*
[c] *Institut Curie, Université PSL, CNRS UMR3347, Inserm U1021, Signalisation Radiobiologie et Cancer, 91898 Orsay, France*
[d] *Medical Physics, University Hospital Birmingham NHS Trust, Mindelsohn Way, Birmingham, B15 2TH, United Kingdom*
[e] *Université Paris-Saclay, CNRS UMR3347, Inserm U1021, Signalisation Radiobiologie et Cancer, 91400 Orsay, France*
[f] *Faculty of Engineering and Physical Sciences, University of Surrey, Stag Hill, Guildford, GU2 7XH, United Kingdom*

E-mail: sam.flynn@npl.co.uk

Abstract: Performing accurate and reliable dosimetry in spatially fractionated beams remains a significant challenge due to the steep dose gradients and microscopic scale of features. This results in many conventional detectors and instrumentation being unsuitable for online dosimetry, necessitating frequent offline validation using radiochromic film.

In this study, the use of a Complementary Metal-Oxide-Semiconductor (CMOS) detector for evaluation of relative real-time dosimetry of proton minibeam radiation therapy (pMBRT) was investigated. The linearity of the CMOS detector was investigated by varying the proton beam current, with a comparison to a PTW 34001 Roos ionisation chamber used to carry out an independent check. It was found that the relative peaks and valleys of the pMBRT beam could be measured, with results comparable to EBT3XD film. The high sensitivity of the CMOS detector meant it was able to measure dose profiles from peak to valley regions, something not possible with the EBT3XD. The CMOS detector was compared to the treatment delivery log files, with correlation in beam position

*Corresponding author.

https://doi.org/10.1088/1748-0221/18/03/P03014

2023 JINST 18 P03014

seen as the beam is scanned along each slit, but not across; and agreement in beam intensity, with the CMOS detector able to observe beam interruptions.

Lastly, the CMOS detector was used in conjunction with the NPL primary-standard proton calorimeter (NPL PSPC) for a preliminary study on combining the NPL PSPC with high resolution temporal information about the incident pMBRT beam. The ultimate aim of this approach is to facilitate detailed thermal modelling to reduce the overall uncertainty in the absolute dose measured from the calorimeter. In these experiments, saturation in the CMOS pixels prevented further thermal modelling of the radiation induced heat flow, however the instantaneous dose rate was observed to be comparable with the predicted NPL PSPC response obtained by masking the CMOS detector.

KEYWORDS: Dosimetry concepts and apparatus; Instrumentation for hadron therapy

2023 JINST 18 P03014

Contents

2023 JINST 18 P03014

1 Introduction

1.1 Spatial fractionation background

Spatial fractionated radiotherapy is a novel form of cancer therapy in which a non-uniform field of radiation is delivered to the tumour [1]. This novel type of therapy is defined by narrow beams of radiation that can selectively irradiate portions of the target volume. In recent years the two forms of spatial fractionation, "microbeam" (typically beams with FWHM $< 100\,\mu m$) and "minibeam" (typically beams with $100\,\mu m <$ FWHM $< 1000\,\mu m$) forms of radiotherapy, have yielded promising results in preclinical experimentation [2, 3]. Spatial fractionation is typically delivered in either a "grid" pattern, with radiation spots regularly distributed in a 2D axis, or via "slits", with multi quasi-parallel rectangular beams.

Spatial fractionation has demonstrated the ability to reduce damage to healthy tissue, whilst maintaining tumour control [4, 5]. The effect associated with spatial fractionation is thought to be the result of contributions of bystander/abscopal effects [6] and induced antitumour immune response [7]. Maintaining tumour control whilst reducing damage to healthy tissue could have

significant impact in how radiotherapy is currently delivered: a reduction in side effects for current treatments; whilst opening up the possibility of radiotherapy for cancers that cannot be currently treated (either due to radioresistence or by being surrounded by vulnerable healthy tissue).

Given the very small fields involved, performing accurate dosimetry in spatially fractionated beams will be significantly more challenging than conventional radiotherapy. To tackle this, a significant amount of research is being conducted globally to develop new techniques, methods, and protocols [8–11]. Two dimensional electronic instrumentation for Stereotactic Radiosurgery (SRS), the closest clinical equivalent treatment, is currently limited in lateral resolution to approximately 0.4 mm [12], much too large for spatial fractionation. The healthy-tissue sparing effect of spatial fractionation is very dependent on how the dose is distributed, an accurate measurement of this dose is required in order to predict the therapeutic outcome. Radiochromic film remains a viable method of dosimetry in spatially fractionated beams [13], however this is time consuming (typically 24-48 hours) and requires off-line analysis and post processing. There is currently no available active detector capable of providing accurate two dimensional real-time measurements of the spatial dose distribution.

1.2 Proton minibeam radiation therapy

Spatially fractionated beams are typically generated by passing a broad beam through a mechanical collimator [14, 15]. Low transmission efficiencies require a large dose rate in order to deliver treatment doses in a reasonable time, restricting their use to large x-ray synchrotron facilities. At the Institut Curie (IC), a technique referred to as pMBRT has been developed [16]. This combines the healthy tissue sparing properties of spatial fractionation, whilst exploiting the Bragg peak of proton therapy to reduce the amount of healthy tissue being irradiated. Preclinical studies have indicated that pMBRT preserves many of the healthy tissue sparing effects of "microbeam" therapy, but without the significant costs and limitations associated with x-ray production from synchrotrons [2, 17–19].

To provide greater confidence in the dose delivered in pMBRT preclinical trials and in preparation for possible future human studies at IC, the NPL PSPC was used to provide the measurement of absolute dose. Due to the dosimetric challenges associated with pMBRT, the uncertainty in dose delivered to the patient is likely to be higher. By using the NPL PSPC it is anticipated that the total uncertainty in dose will be lower.

1.3 Primary standard calorimetry background

An ongoing concern for primary standard calorimetry is the effect of internal heat-flow within and between the graphite components. Although best efforts during design and construction are made to thermally isolate the internal components; thermal pathways exist between the graphite core and the surrounding "*jackets*" via thermal conduction and radiative heat transfer. The quantity of interest requiring measurement is the radiation induced temperature rise of the graphite, which is ascertained by small thermistors embedded in the core. If thermal energy is transferred to the core from the surrounding "jackets", the NPL PSPC will over-respond. Likewise, if thermal energy is lost from the "core", the NPL PSPC will under-respond. In a passively scattered proton beam, it is assumed that internal heat flow is negligible as the core and jackets are being irradiated at the same time. This is not the case for scanned pencil proton beams, where a rapidly moving proton beam causes non-uniform heat flow.

Thermal modelling within the NPL PSPC, as conducted by Petrie [20] and Flynn [21], is required to compensate for this induced heat flow. Whilst it is possible to correct for internal

2023 JINST 18 P03014

heat flow using Finite Element Model (FEM) software, due to insufficient knowledge of how each beam is spatially and temporally delivered, calculating the corrections needed is not possible on a per delivery basis. Instead an additional uncertainty of 0.41% ($k = 1$) is applied to all dose measurements [22]. This is the second largest component in the uncertainty budget [22], and impacts all clinical calibrations and comparisons.

It may be possible to reconstruct the incident beam using planning logs, however as a primary standard level instrument this is not an option because it may inherit biases or errors. The NPL PSPC must be independent from the beam delivery system. Prior studies have demonstrated the potential of a combined system [21], however it has not been demonstrated in a proton beam facility.

Concerns regarding internal heat-flow are magnified in spatially fractionated beams where the radiation is delivered non-uniformly across the core. Additionally, the position of the calorimeter (relative to the beam delivery coordinates) is especially important as small variations in position will influence the number of pMBRT peaks interacting with the NPL PSPC core.

As part of the research objectives for improving the understanding of the NPL PSPC, a proof-of-principle investigation was carried out with the CMOS detector to characterise the detector in pMBRT beams.

2 Materials and methods

2.1 CMOS detector

The vM2428 detector, also referred to as *Athena* or *LASSENA* [23], is a large-format Complementary Metal-Oxide-Semiconductor (CMOS) sensor designed for scientific and medical x-ray imaging. Although it was not designed for pMBRT, previous investigations at University College Hospitals London NHS Foundation Trust (UCLH) [24] have demonstrated that the detector was a viable candidate for use with proton beams, whilst the precursor to the vM2428 detector, the vM1212 detector, was found to be able to measure static and dynamic x-ray microbeams in a Small Animal Radiation Research Platform (SARRP)[25, 26]. The vM2428 detector's specifications are described further in table 1.

Table 1. Specifications of the vM2428 detector.

Name	Quantity	Units
pixel pitch	50	µm
resolution	2400×2800	pixels
active area	120×140	mm^2
minimum integration time (full frame)	28.3	ms
digital resolution	2^{14}	bits

At IC, the proton beams are generated using a 230 MeV C235 IBA proton cyclotron connected to two treatment rooms that have passively scattered beams and a third treatment room that has pencil beam scanning (PBS) [27]. In the room with PBS, proton minibeams are created using a 6.5 cm thick brass collimator with slits with variable slit parameters machined into it. By changing the collimator, the operators are able to easily change slit width, length, and separation; although

2023 JINST 18 P03014

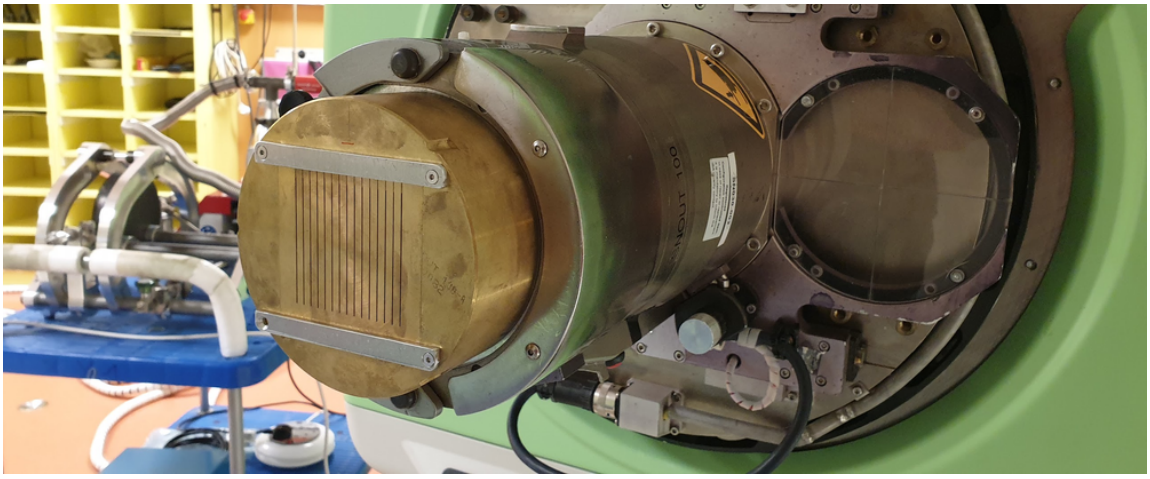

Figure 1. Photograph of the minibeam collimator attached to the beam nozzle, showing the machined 400 µm slits.

similarly to passively scanning collimators these must be machined in advance. A photograph of a minibeam collimator is shown in figure 1. Further specification of the collimator design is available in [28].

The vM2428 detector was investigated at IC on two separate occasions, separated by approximately 5 months: (i) a focus on the ability of the vM2428 detector to measure proton minibeam profiles, with a focus on comparison with radiochromic film; (ii) to provide support for an investigation with the NPL PSPC.

2.2 NPL proton calorimeter

The NPL PSPC is a primary standard level instrument, designed to measure absorbed dose to graphite (d_g) in passively scattered proton beams and scanned proton pencil beams [22, 29]. Thermistors embedded within the core and surrounding jackets are connected in networks to provide temperature sensing or electrical heating. For a typical radiation dose fraction of 2 Gy, the corresponding temperature increase in graphite is less than 3 mK. To measure these small temperatures at high accuracy, each sensing thermistor network is configured with its own DC Wheatstone Bridge circuit and high precision nano-voltmeter.

The NPL PSPC is designed based on a "Domen" style configuration [30], with a graphite core (a 2 mm thick, 16 mm diameter disc) surrounded by several thermally isolating graphite jackets. The sensitive volume of the core has been chosen to match the collection volume of a PTW Roos plane-parallel ionisation chamber [31]. Two thermistors are embedded midway between the front and rear surface in the sidewall of the core, 1 mm below the surface of the graphite. These are referred to as "Core 1" and "Core 2", serving as primary temperature sensor for dose measurements and the secondary temperature sensor for redundancy, respectively. This configuration is shown in figure 2, and is intended for horizontal beam delivery.

2023 JINST 18 P03014

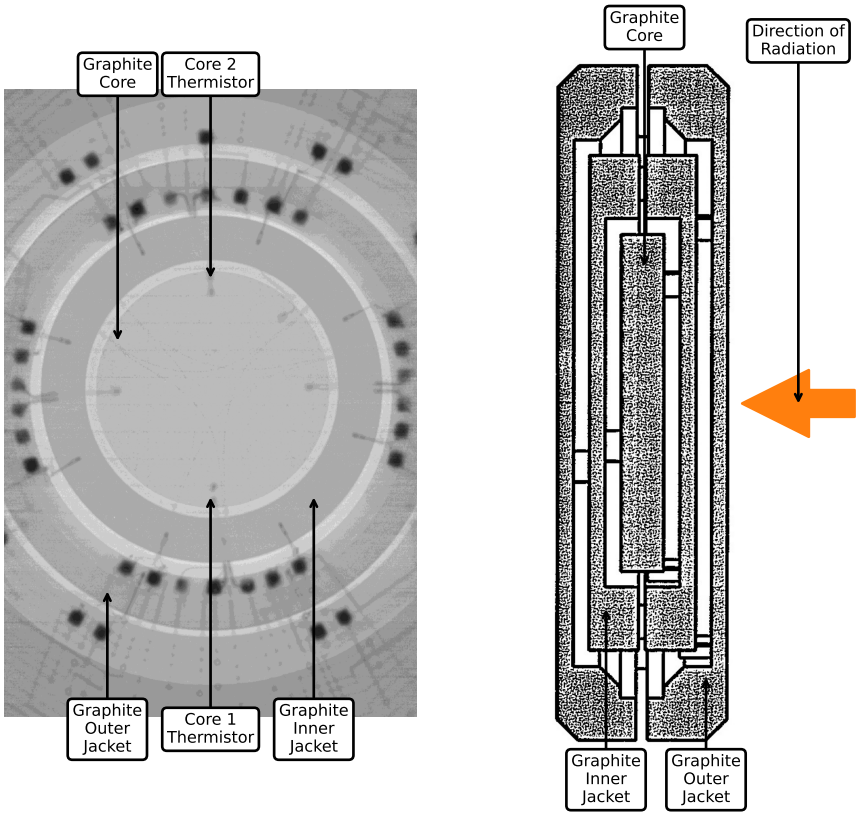

Figure 2. Geometric configuration of the NPL PSPC: (Left) Annotated radiograph of the "core" showing the relative position of the two sensing thermistors. (Right) Annotated engineering diagram of the NPL PSPC showing a cross-sectional view.

3 CMOS detector characterisation in proton minibeams

3.1 Methodology

For the dedicated CMOS experiment, the vM2428 detector was positioned on the treatment couch for a beam pointing vertically downwards (gantry 0°). Whilst previously a horizontal beam was required to measure the same beam as the NPL PSPC, a vertical beam dramatically simplifies the setup required for the CMOS studies. The detector was positioned on top of an ABS block to facilitate cable management, which, in-turn, was placed on top of a slab of WTe [32]. A PTW 34001 Roos ionisation chamber [31] (serial number 2898) was inserted into the WTe solid water, with a small WTe disc, positioned in the hollow rear face to remove the air gap.

The centre of the vM2428 detector was aligned to the centre of the beam using the isocentre lasers; then the height of the treatment couch was adjusting such that the surface of the vM2428 detector was positioned 7 cm from the front face of the collimator, corresponding to the reference conditions at IC. The readout Printed Circuit Board (PCB) was placed on the treatment couch, separated from the active area by 20 cm of ribbon cable to minimise radiation damage from scattered radiation. A photograph of the setup can be seen in figure 3.

2023 JINST 18 P03014

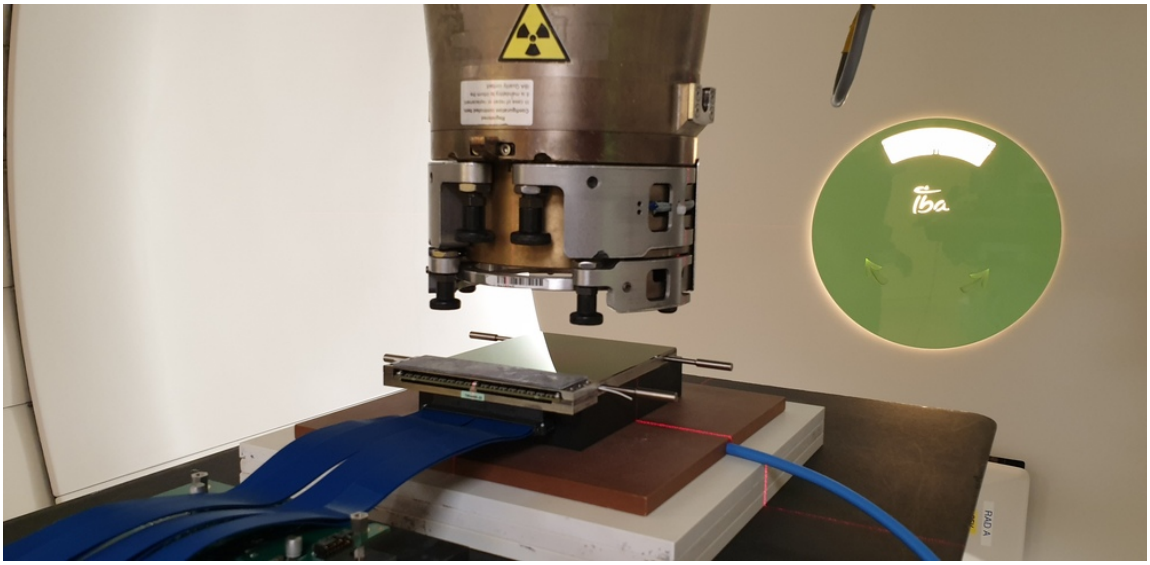

Figure 3. Photograph of the vM2428 detector during setup, positioned 7 cm from the surface of the collimator.

3.2 Linearity study

To measure profiles and parameters using the vM2428 detector, the raw Analogue-to-Digital Units (ADU) from the CMOS output first needed to be linearised and calibrated in the 100 MeV beam. For imaging applications a conversion is to e^-/ADU is typically performed [33], however for radiation dosimetry applications Gy/ADU (absorbed dose per ADU) is desirable. Whilst no significant change to the response curve was expected relative to the previous measurement at UCLH (220 MeV), the differences in stopping power between the beams, and beam pulse structure necessitated additional investigation.

The linearity and calibration were performed by irradiating the sensor with stationary single proton beams (FWHM determined to be 21.1 ± 0.1 mm using the vM2428 detector) without collimation for approximately 15 seconds at several beam currents. This beam was positioned in the centre of the active area of the CMOS, with an estimated positioning uncertainty of ±2 mm [34]. The radiation beams were measured simultaneously on both the vM2428 detector and the PTW Roos chamber, allowing a linearisation to be performed. A Flat-Field Correction (FFC) was applied to the CMOS using prior measurements from a diffuse light box to account for non-uniformity of the vM2428 detector [21]. The charge measured with the Roos chamber was converted to average beam current using temporal information about the beam on/off position using the vM2428 detector signal (shown in figure 4).

Although the Roos chamber was calibrated in terms of Gy/nC, lateral Charged Particle Equilibrium (CPE) was not achieved, and as such a conversion to Gray from the measured signal could not be performed without a significant amount of Monte Carlo simulations, which are beyond the scope of this project at this time. Despite this, the response of the vM2428 detector can be seen in terms of relative dose by appropriate normalisation, as discussed in subsections 3.3 and 3.4.

To prevent saturation of the vM2428 detector in the proton minibeams, a narrow Region Of Interest (ROI) was applied to the vM2428 detector of 300 rows to reduce the integration time to 3.13 ms per frame. Linearity measurements were performed at 12.5%, 25%, 37.5%, 50%, and 100%

2023 JINST 18 P03014

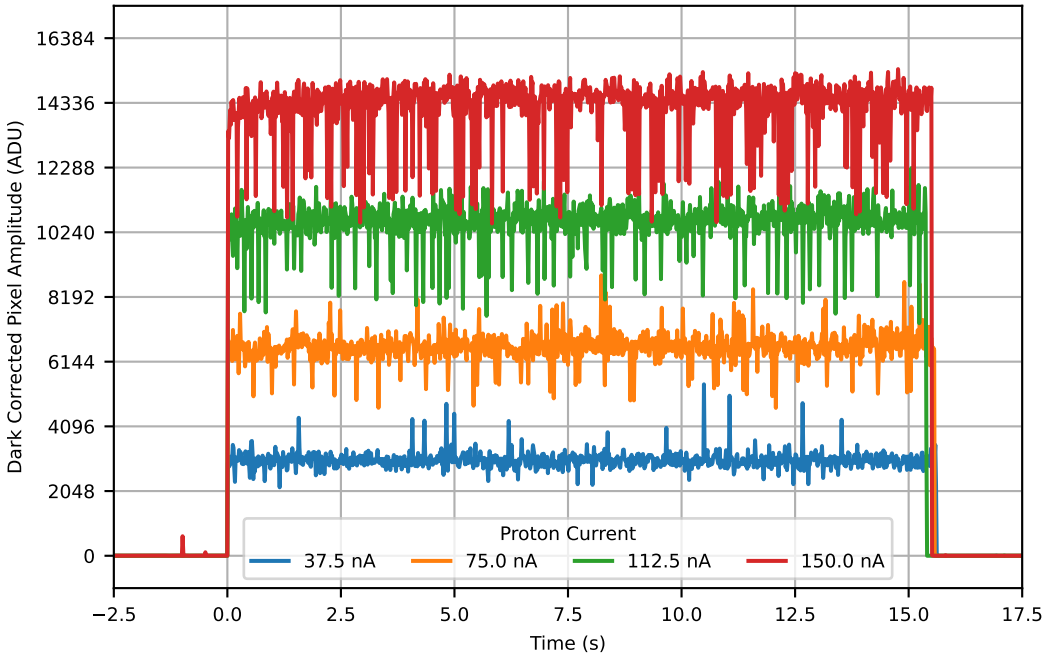

Figure 4. Average pixel amplitude of various proton beam current as measured by the vM2428 detector.

fractions of the clinical beam current of 300 nA without a collimator applied. Although saturation was observed in these linearisation measurements above 37.5 nA, this was determined not to be an issue when using the proton minibeam collimator as the low transmission efficiency reduced the instantaneous dose rate observed in the minibeam peaks. Although a row-skipping functionality was available in the firmware of the CMOS detector to further reduce the integration time, it was not selected for this series of measurements due to an incomplete characterisation of the behaviour and impact upon the sensor.

The average response in the central 10×10 pixels of the vM2428 detector was fitted to a hybrid linear-exponential model to account for both the linear region of non-saturation and the saturated plateau, as described in Equation 3.1. The proton current (x) is given as a function of the dark corrected ADU value (y); the coefficient (a) which controls the gradient during the linear region; the coefficient (b) which controls the magnitude of the exponential term; the coefficient (c), which corresponds to the exponential growth (and thus saturation of the pixel); and the coefficient (d), which determines the inflection point at which saturation occurs.

$$x(y) = ay + be^{c(y-d)} - be^{-cd} \tag{3.1}$$

The linearisation of the vM2428 detector can be seen in figure 5, where a linear response was observed up to 34 nA current in the ionisation chamber. This observed response is consistent with the prior CMOS measurements [24].

Unlike prior measurements with the vM2428 detector carried out at other proton beam facilities [24], it was found that the IBA Cyclotron was very stable at a variety of beam currents. This is shown in figure 4, although the beam stability is observed to decrease at higher beam current.

2023 JINST 18 P03014

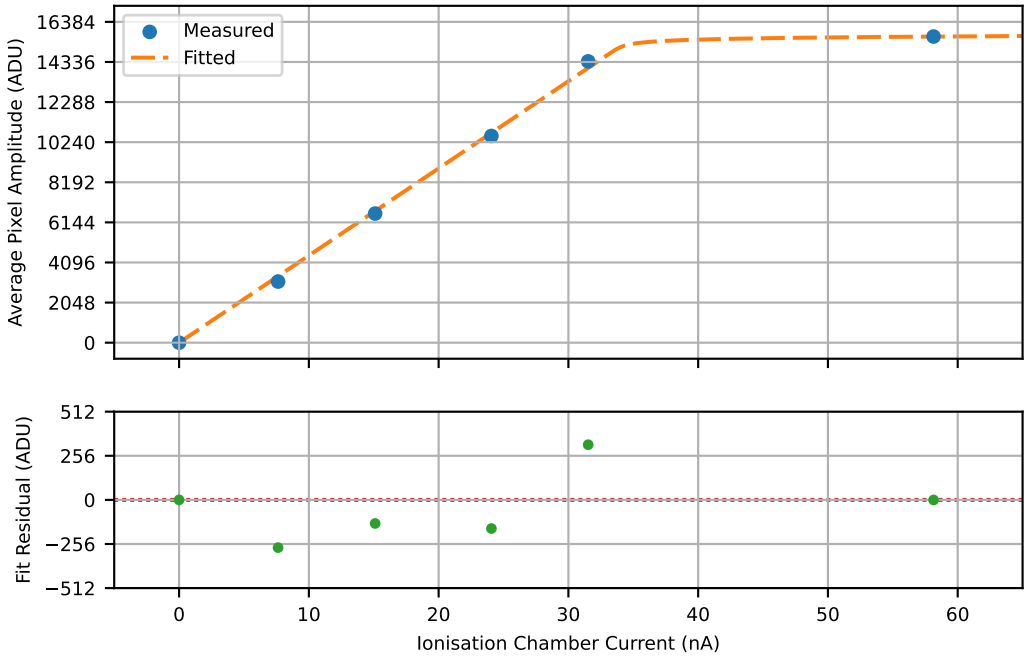

Figure 5. Calibration measurements of the vM2428 detector in a monoenergetic 100 MeV proton beam against a Roos chamber positioned downstream from the CMOS detector.

3.3 Single spot study

For the first part of the investigation, a collimator with 5 cm long × 400 µm wide slits with 4 mm centre to centre separation was attached to the gantry to create the pMBRT delivery pattern. The treatment delivery system was configured to deliver a 100 MeV beam to a single position in the centre of the vM2428 detector; aligned with the PTW Roos chamber. Although this is not a delivery used at the Institut Curie (IC) for preclinical research, it was chosen to allow evaluation of the dose response of the vM2428 detector in complex radiation fields.

A sheet of EBT3XD [35] radiochromic film was placed directly on top of the active area of the CMOS. This was scanned as 300 dpi at IC and calibrated using a 14 point dose scale between 0-50 Gy (0, 0.25, 0.5, 1, 2, 3, 4, 5, 6, 8, 10, 15, 30, and 50 Gy dose values). A comparison of the EBT3XD film and a single vM2428 detector frame 2D profiles, both normalised to the central peak is shown in figure 6.

Gamma evaluation is a clinically used method of performing quality assurance measurements to compare a delivered radiation plan to a reference plan (typically from a TPS) [36]. It represents a quantitative method of determining how geometrically close each pixel is to the reference pixel of the same value, and the percentage difference between two pixels in the same geometric location. A gamma value greater than 1.0 is considered a failure, with anything less than 1.0 considered a success.

At the time of writing there is no agreed upon protocol for gamma evaluation for spatially fractionated beams delivery (although several recommendations have been published [10, 37]). To compare the two detectors, a 5%/0.5 mm local gamma analysis based on Stereotactic Radiosurgery (SRS) recommendations was chosen [38]; with EBT3XD film used as the reference plan. A 1% dose

2023 JINST 18 P03014

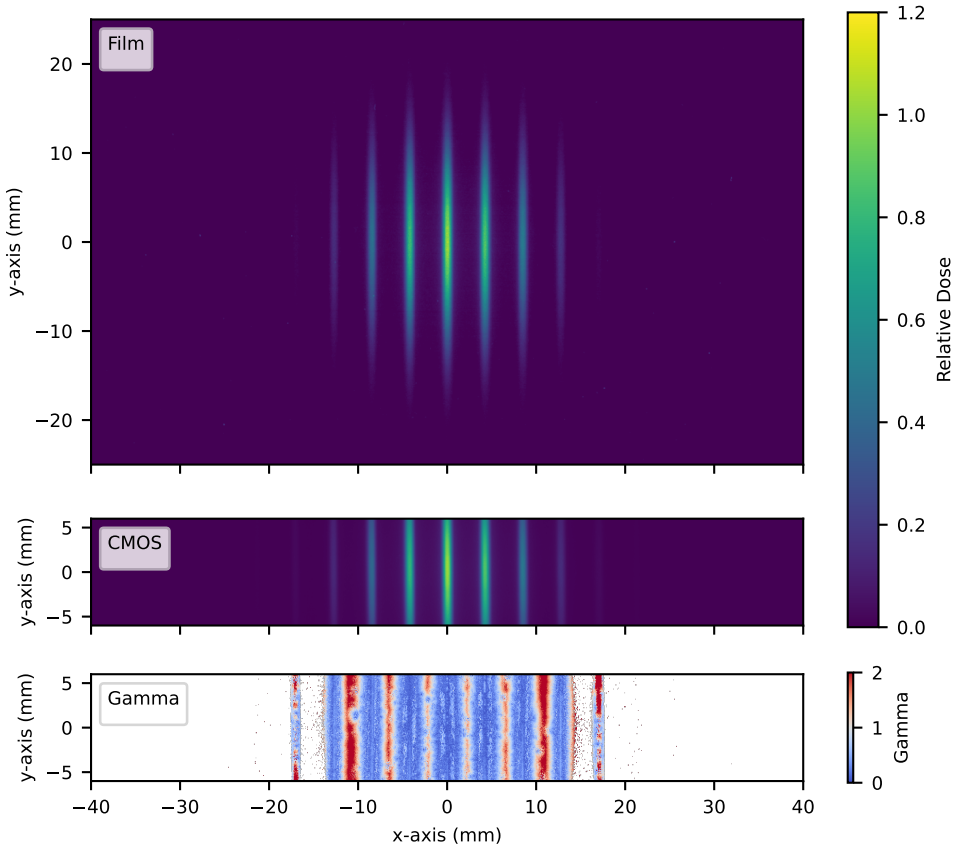

Figure 6. Normalised single pMBRT beam comparison of EBT3 film (top), a single vM2428 detector frame (middle) and gamma analysis (5%/0.5 mm) (bottom).

threshold was chosen in order to better measure the minibeam valley regions, as recent evidence highlights the importance of dose delivered to this region for optimising pre-clinical outcomes [39]. Gamma analysis was conducted using the PyMedPhys library [40].

The gamma passing rate was determined to be 73.4%, with analysis of the 2D distribution (figure 6) highlighting that the EBT3XD appears to under-respond to the minibeam valleys. A one dimensional profile comparison of a single vM2428 detector frame to the EBT3XD film is shown in figure 7.

The measured FWHM of the central peak was determined to be 1.21 ± 0.01 mm using the CMOS, and 1.24 ± 0.01 using the EBT3XD film. This again shows good agreement in the minibeam peaks, but not in the minibeam valleys. This results in a large discrepancy between the measured Peak-to-Valley Dose Ratio (PVDR), a quantity of interest within spatial fractionation [41, 42], with the CMOS is measuring approximately 20, whilst the EBT3XD measured PVDR is over 33. The vM2428 detector is also able to observe low dose minibeam peaks at distances greater than ± 15 mm, something the EBT3XD is not able to measure.

This is most likely due to the EBT3XD film receiving less than 0.2 Gy in the valley regions immediately after the central peak, with valley doses indistinguishable from background after the 2nd most inner peak. This is significantly less than the 0.4 Gy limit suggested by the film

2023 JINST 18 P03014

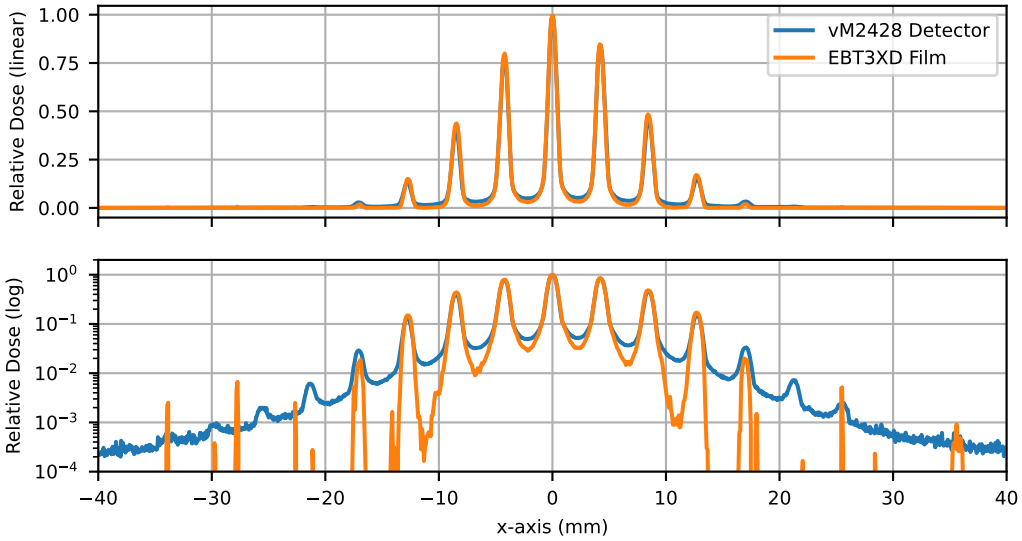

Figure 7. Horizontal profile comparison of EBT3 film and a single vM2428 detector frame for a single beam spot. The relative dose for vM2428 and the EBT3XD film is presented in linear scale (top diagram) and logarithmic scale (bottom diagram) to emphasise the differences between two measurement methods.

manufacturer [43], and the film response would be especially sensitive to any slight miscalibration in this region. This again highlights the versatility of sensitive CMOS detectors for measurement of low dose valleys as previously demonstrated for x-ray microbeams [25].

The gamma passing rate for the average of all vM2428 detector frames is 73.2%, indicating that random noise does not contribute significantly to the CMOS detector's ability to measure pMBRT profiles. These results indicate the feasibility to employ the vM2428 detector as a real-time verification tool for spatially fractionated beams.

A comparison of different gamma evaluation criteria for the single spot comparison can be seen in table 2.

Table 2. Gamma Evaluation of the vM2428 detector against EBT3XD film for single and multi spot fields.

Gamma Criteria	Single Spot Field (%)	Multi Spot field (%)
3%/3 mm	82.0	82.7
2%/2 mm	73.5	79.0
1%/1 mm	58.6	74.2
0.5%/0.5 mm	43.3	67.9
5%/ 0.5 mm	73.2	83.8

3.4 Scanned Spot Study

The treatment delivery system was then configured to deliver a $7 \times 7\,\mathrm{cm}^2$ monoenergetic (100 MeV) field, delivering a total of 12500 MU at 300 nA beam current. A comparison of the EBT3XD and vM2428 detector response in two dimensions can be seen in figure 8, again normalised to the central

2023 JINST 18 P03014

slit maximum. For direct comparison with the previous section (section 3.3), the same ROI was chosen on the detector.

As the beam is scanned across the EBT3XD film and vM2428 detector, to create a cumulative profile for analysis it is not possible to compare individual frames; instead the comparison must be to the average of all CMOS frames during the delivery.

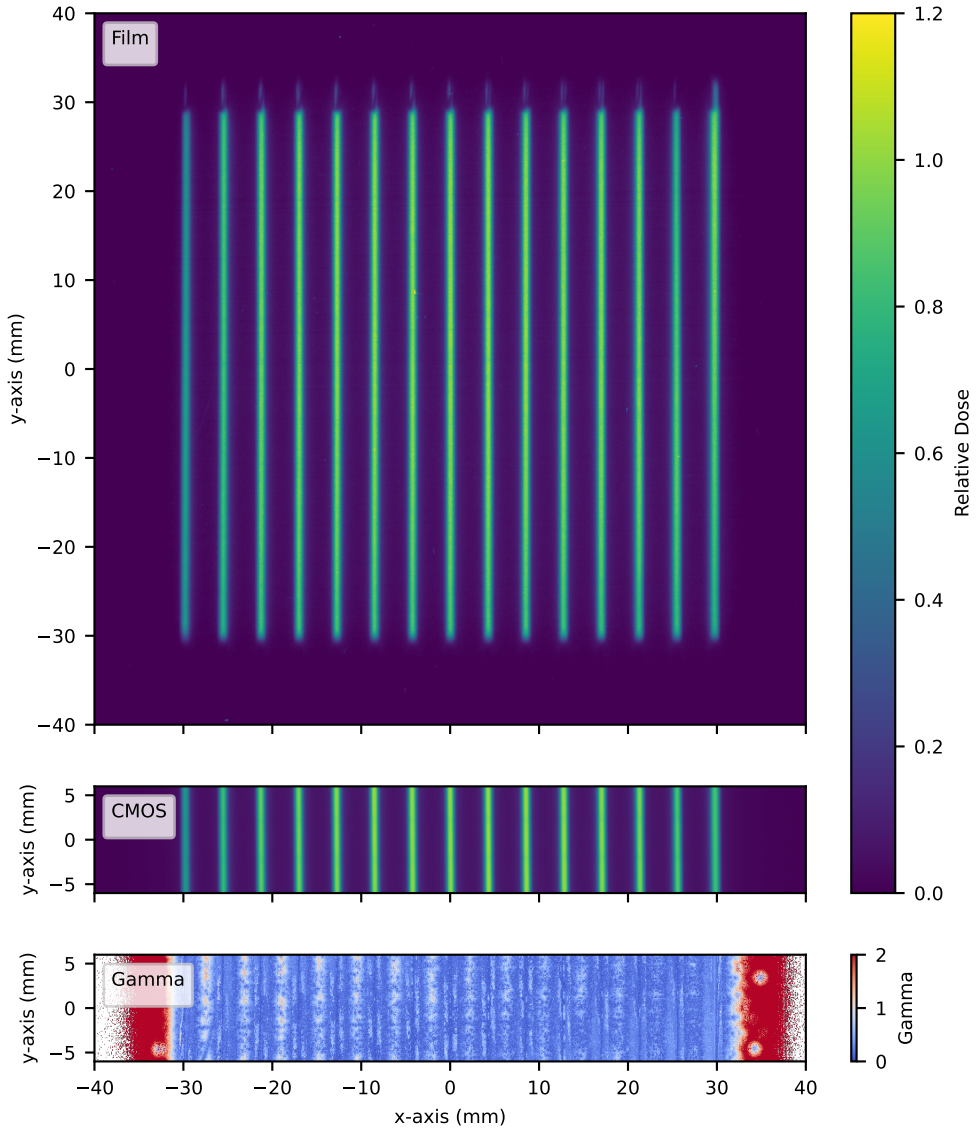

Figure 8. Normalised multi spot pMBRT beam comparison of EBT3 film (top), a single vM2428 detector frame (middle) and gamma analysis (5%/0.5 mm) (bottom).

Conducting a gamma analysis, 5%/0.5 mm (local), of the data presented in figure 8 produces the lower image in figure 8. Here, it can be shown that there is agreement between the two detectors, including the valley regions, with the only regions of gamma failure being in the beam penumbra. The gamma passing rate is determined to be 83.8%, significantly higher than the single beamlet.

2023 JINST 18 P03014

The minimum dose in the EBT3XD film valleys is approximately 0.5 Gy, much greater than in section 3.3. This provides supporting evidence that prior disagreement was due to uncertainties in the EBT3XD film response at low doses and possible miscalibration in the film response at these positions.

A horizontal profile comparison between the two detectors can be seen in figure 9, highlighting much better agreement in both the dose peak and valley regions than the single beam plot. The average PVDR in the CMOS measurement is 14.32 ± 1.08 (k = 2, Type A uncertainty), whilst it is a slightly higher 17.23 ± 1.96 (k = 2, Type A uncertainty) for the EBT3XD film. Fitting a Gaussian to each of the peaks finds the FWHM measured by the CMOS and the EBT3XD to both be 1.19 ± 0.06 mm (k = 2, Type A uncertainty).

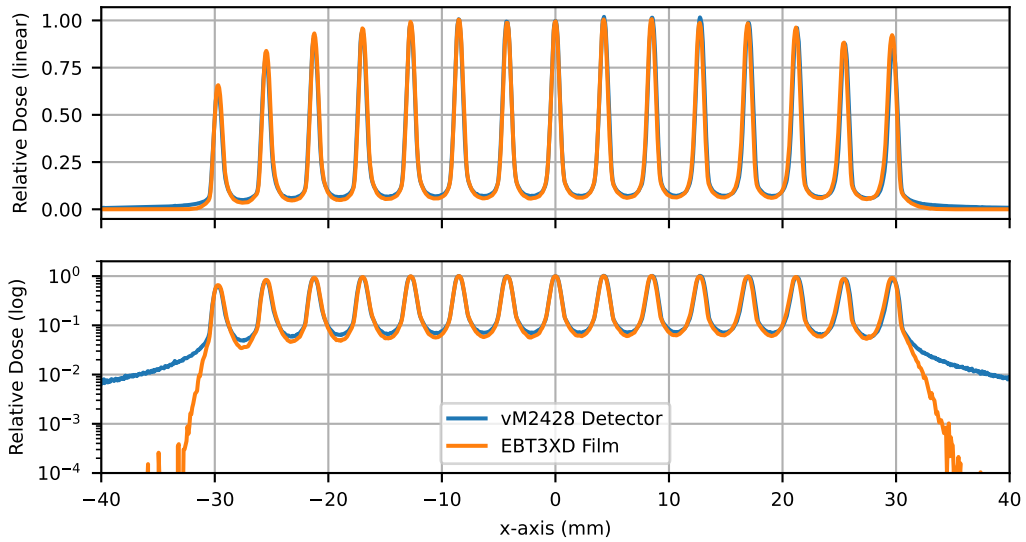

Figure 9. Horizontal profile comparison of EBT3 film and a single vM2428 detector frame for a multi-beam spot. The data is again presented on a linear and a logarithmic scale to emphasise between the two measurement methods.

A comparison of different gamma evaluation criteria for the multiple spot comparison can be seen in table 2.

Increasing the ROI to the full active area increases the integration time of the detector, causing saturation, but allows for visualisations of the dose deposition to be created.

Analysis of the moving beam was conducted. To account for saturation, an array mask (figure 10) was applied to each frame of the CMOS to remove the beam information in the peak regions. This resulted in only the valleys doses available for analysis, and future implementations of this analysis would ideally be using non-saturated data.

As shown in figure 11, the beam position pattern determined with vM2428 detector has good agreement with the treatment log files in the x-axis, along the slits, but not in the y-axis where the orientation is tangential. The beam centre position in the y-axis, as determined by the CMOS is observed to have a ringing effect, and is attributed to geometric scattering through the collimator. When scanning in the opposite direction (not shown for brevity), the same ringing pattern is observed,

2023 JINST 18 P03014

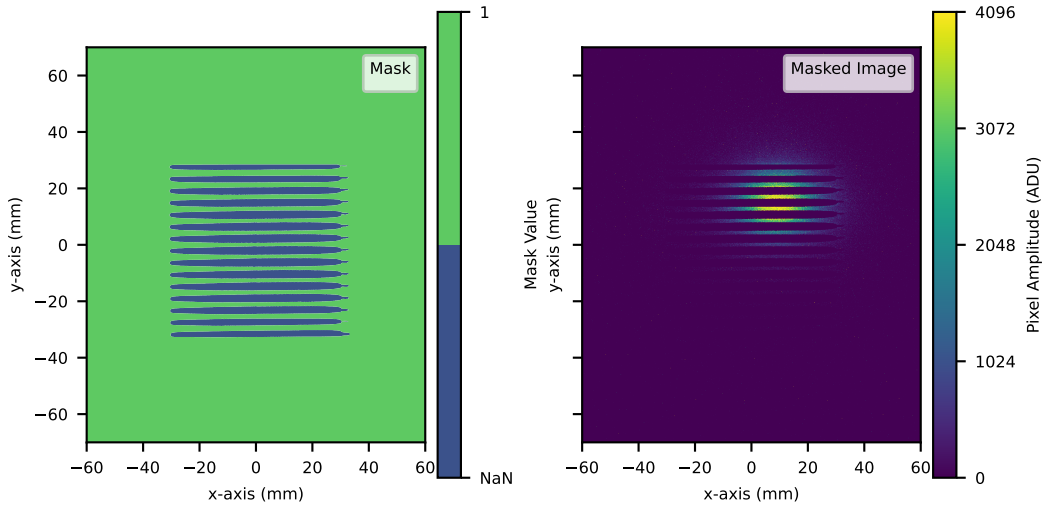

Figure 10. (Left) Mask applied to vM2428 detector to remove saturation of the beam from the pMBRT peaks. (Right) Masked image from the vM2428 detector. For visual clarity, the masked regions have been set to zero however in the analysis they are set to NaN.

however swapped between the x and y axes. This ringing pattern is likely a limitation of using a centre of mass function to calculate the beam centre.

The vM2428 detector measured positions were larger than those from the treatment log files, attributed to the different positions of the strip detectors composing the treatment log files and the CMOS; and taking into account beam divergence.

It can be seen that the relative dose rate of the TPS is consistent throughout the exposure, this is to be expected as the measurement system is before the collimator and as such would be measuring a pristine pencil beam. An important observation is that the beam paused at approximately 40 seconds into the delivery, due to a 10000 MU limit being reached (see figure 11).

4 Support for calorimeter study

4.1 Methodology

A separate investigation at IC provided the opportunity to compare the CMOS sensor with the NPL PSPC. Due to practical space limitations and time constraints, it was not possible to investigate irradiating both instruments at the same time.

For this setup the vM2428 detector was suspended vertically, standing on the treatment couch using a custom frame with the PCB and readout electronics above the sensitive area out of the beam. The surface of the CMOS detector was horizontally moved such that it was 7 cm from the surface of the proton minibeam collimator, at IC reference conditions. A water phantom was used behind the CMOS detector as a beam dump. This setup can be seen in figure 12.

Additional graphite was placed in front of the calorimeter to position the centre of the core at a water equivalent thickness (WET) of 2 cm. This build-up is required in order to place the "core" of the NPL PSPC at a specific depth within the graphite, where Charged Particle Equilibrium has

2023 JINST 18 P03014

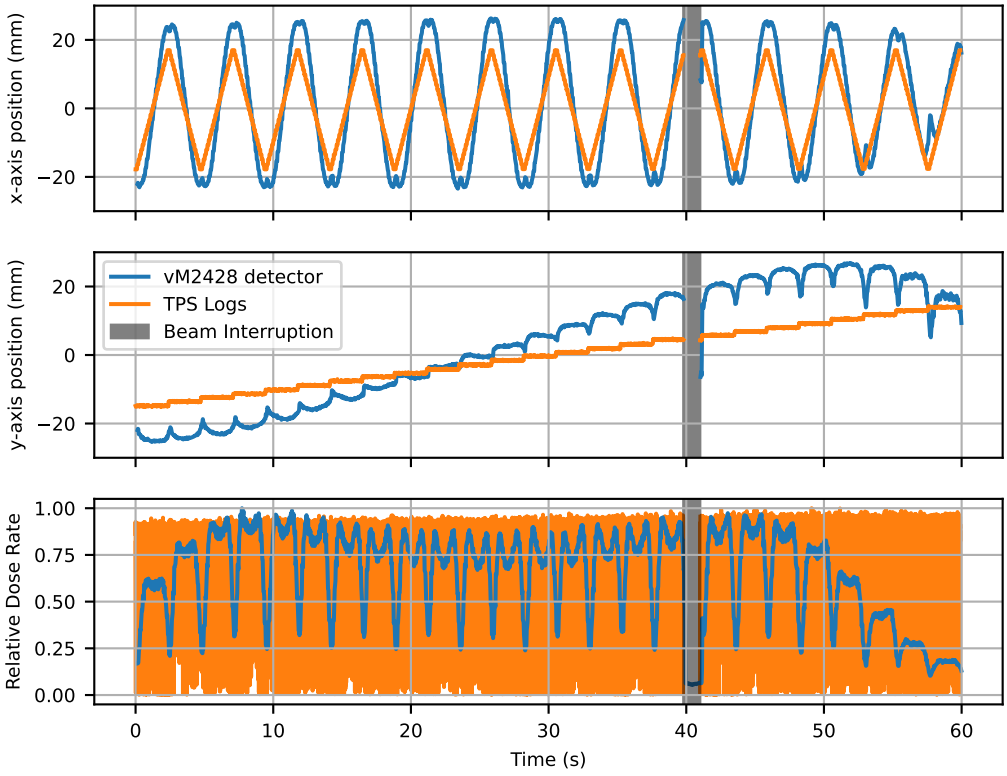

Figure 11. Comparison of beam positions and relative dose rate using the vM2428 detector and the TPS logs x and y axis. Note the interruption in the beam delivery at approximately 40 seconds.

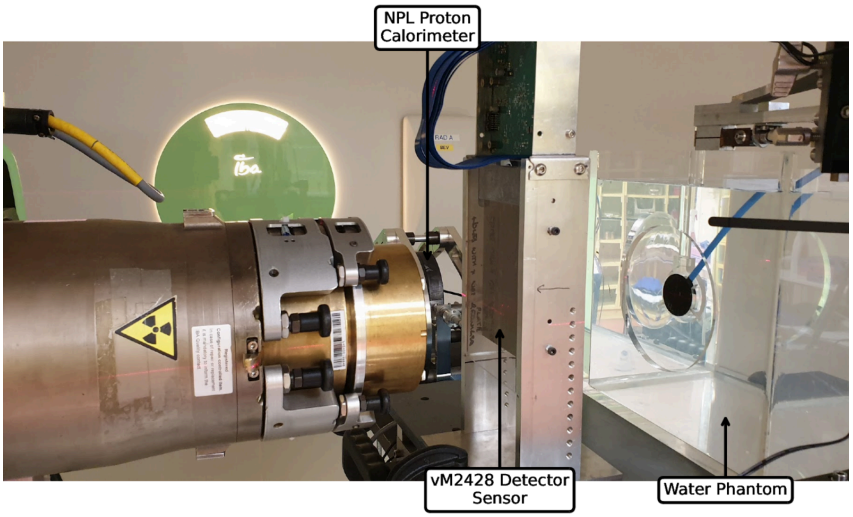

Figure 12. Annotated Diagram of the vM2428 Detector setup.

2023 JINST 18 P03014

been achieved. The calorimeter, operating in quasi-adiabatic mode, was exposed to 15 consecutive irradiations of 12500 MU, with a 3 minute delay between each irradiation to allow for thermal settling. Due to the protruding metal frame which supports the calorimeter's graphite components, the NPL PSPC had to be vertically offset from the centre of the beam by 11 mm, in order to achieve the 7 cm separation from the surface of the collimator. This provided the clearance required to avoid irradiation of the calorimeter support frame.

4.2 Results

Preliminary results indicate that the mean dose to core from a 100 MeV multi spot pMBRT beam was 1.80 ± 0.15 Gy, ($k = 2$, Type A uncertainty). In the future, it is planned to calculate the remaining Monte Carlo corrections to enable determination of dose to graphite and dose to water.

Analysis of the instantaneous dose rate, as determined by the two core thermistors, can be seen in figure 13. To account for electrical noise in the study of heat-flow, the average instantaneous dose rate across all 15 runs is shown. A positive dose rate is a result of a combination of radiation induced temperature increase and heat-flow into the thermistor from the calorimeter core, whilst a negative dose rate corresponds to thermal energy being transferred into the graphite core from the thermistors.

Due to the core thermistors being physically separated from each other, the instantaneous dose rate is different as the pMBRT beam is scanned across the calorimeter. This is consistent with prior tests in moving x-ray beams [21]. As the "Core 2" thermistor is shown to have a larger negative dose rate than the "Core 1" thermistor, it can be surmised that it is more directly irradiated by a scanned proton beam.

The average pixel response in the core area of the CMOS detector was determined by masking out all pixels, except those over the NPL PSPC core (figure 14). The average response in this region is thus used to make predictions on the calorimeter heat-flow, however due to the saturation observed by the pixels this is limited to qualitative analysis at present.

Full analysis of the NPL PSPC in pMBRT is beyond the scope of this paper and will be the subject of a standalone article in the future, however it is important to note that the response in both instruments correlates. The results obtained infer that the vM2428 detector responds to peaks from the scanned beam as it is scanned before the thermistors. This is due to a combination of factors: the vM2428 detector measuring primary and secondary particles in air, whilst the thermistors are embedded deep within graphite requiring direct irradiation. Additionally, as shown in figure 13, the noise floor of the instantaneous dose rate measurements obscures any radiation not centred on the core. The point at which the instantaneous dose appears to rise (approximately 17 seconds) corresponds to the first point at which both the x and y-axis position of the beam are within the region occupied by the calorimeter core. A small rise is visible on the CMOS at approximately 12 seconds, however this is not visible on the instantaneous dose rate figure due to noise.

As with the previous tests there is a beam interruption at approximately 40 seconds. The delay in beam delivery due to the interrupt is repeatable, and was observed to vary for between 1.2 ± 0.1 seconds (as determined using the signal decrease using the CMOS detector measurements). This is observed on the instantaneous dose rate plot as a large increase in the standard deviation in both thermistors.

2023 JINST 18 P03014

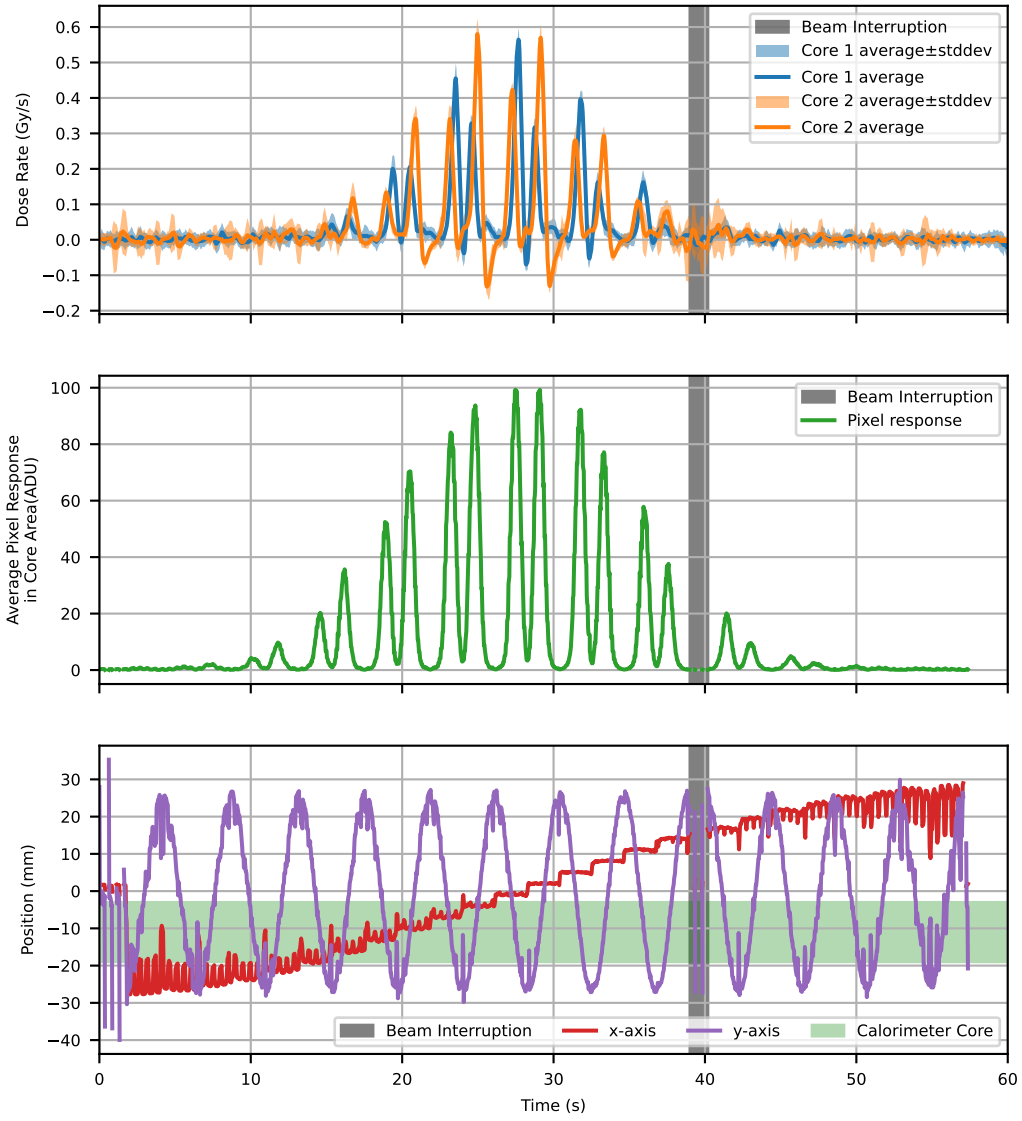

Figure 13. Instantaneous NPL PSPC response against raw vM2428 detector response and beam position, highlighting the correlation between the two instruments. An instantaneous dose rate is observed on the NPL PSPC (top figure) when the beam is scanned over the NPL PSPC core region (bottom figure). This behaviour is replicated on the CMOS detector (middle figure). A temporal difference is observed between the "*Core 1*" and "*Core 2*" thermistors, due to dose deposition over the thermistors.

5 Discussion

Performing accurate on-line dosimetry in pMBRT remains a significant challenge, and whilst the results presented in this paper address some of this; the current pixel saturation remains an obstacle. As the design of the vM2428 detector pixels were optimised for x-ray imaging, the electron full well capacity of the pixels reflects this. Implementing row-skip functionality into the detector could address saturation, but would compromise the vertical resolution of the CMOS.

2023 JINST 18 P03014

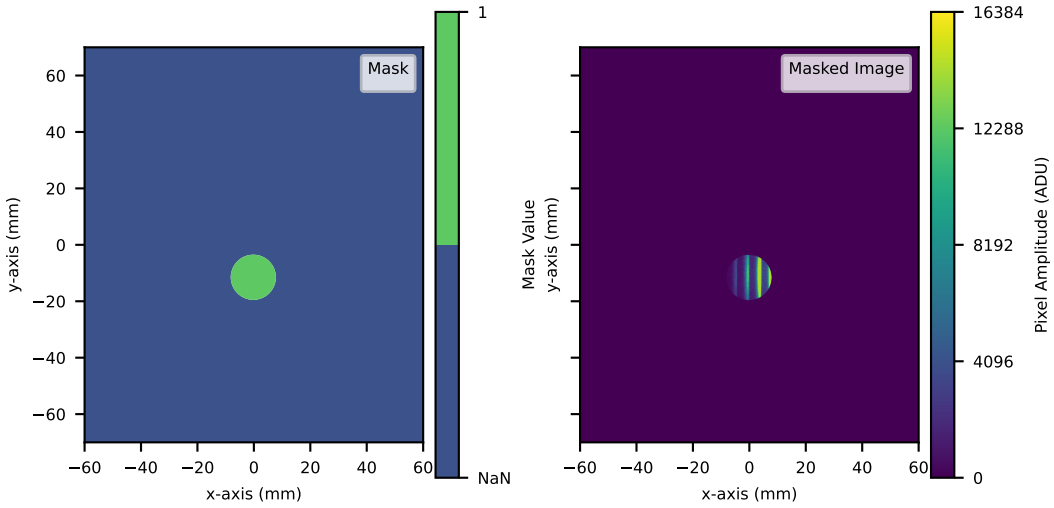

Figure 14. (Left) Mask applied to vM2428 detector to represent the NPL PSPC core. (Right) Masked image from the vM2428 detector. For visual clarity, the masked regions have been set to zero however in the analysis they are set to NaN.

As discussed in section 1, the NPL has a long-term objective to combine the NPL PSPC with a PSD, and this test is a major step towards achieving this. With information such as beam position, shape, and intensity as a function of time; a combined system composing of both the NPL PSPC and a PSD would reduce the uncertainty in measured dose. As demonstrated in section 4, high resolution temporal and spatial information from a CMOS detector could account for beam interruptions; allowing for a per-beam internal heat-flow correction factor with a lower uncertainty of the measured dose. Further study of the hypothesised rotational misalignment could be performed by accurately rotating the CMOS detector and repeating the investigation at different angles. Following this validation of the vM2428 detector, additional tests are planned to simultaneously irradiate both the NPL PSPC and the CMOS sensor.

Full analysis of the internal thermal energy transfers would require a significant amount of finite element modelling combined with Monte Carlo modelling. With saturation observed in the detector for full frame measurements, the capability to perform an in-depth analysis of three dimensional pMBRT is not available at present.

A future objective is to perform a systematic comparison of conventional dosimetry equipment to the CMOS in pMBRT with an ambition of integrating the vM2428 detector into a scanning water phantom. This would enable high resolution 3D dose measurements in water, something that is currently impossible with existing conventional equipment and would allow for a thorough comparison against Monte Carlo beam models.

6 Conclusion

In this paper, it has been demonstrated that CMOS detectors could potentially be used to assist with quality assurance tests for pMBRT, comparable to EBT3XD. The pixel pitch of 50 µm is adequate

2023 JINST 18 P03014

for measuring the intense dose gradients in the spatially fractionated beam; however the limited full well capacity necessitates the implementation of a narrow ROI to prevent saturation.

A correlation between CMOS detector response and instantaneous dose rate in the NPL primary-standard proton calorimeter (NPL PSPC) has been observed, however due to saturation it is not possible to incorporate the data into a Finite Element Model (such as COMSOL [44]).

Acknowledgments

This project 18HLT04 UHDpulse has received funding from the EMPIR programme co-financed by the Participating States and from the European Union's Horizon 2020 research and innovation programme. This project received funding (Y. Prezado) from the European Research Council (ERC) under the European Union's Horizon 2020 research and innovation program (Grant Agreement No 817908). The authors are grateful and wish to thank Mohammad Hussein at the National Physical Laboratory for his thoughts and suggestions regarding appropriate Gamma analysis criteria.

Conflict of interest. Due to the prototype nature of the vM2428 detector, the manufacturer Nordson provides technical support and advice where appropriate upon request.

CRediT Author Statement. A Contributor Roles Taxonomy (CRediT) author statement [45] is provided in table 3.

Table 3. Table representing CRediT author statement.

Author	Conceptualization	Methodology	Software	Validation	Formal analysis	Investigation	Resources	Data Curation	Writing - Original Draft	Writing - Review and Editing	Visualization	Supervision	Project administration	Funding acquisition
Samuel Flynn	x	x	x	x	x	x	x	x	x	x	x	x		
Philip Allport							x			x				
Ludovic De Marzi	x	x	x		x	x	x	x		x		x		x
Stuart Green							x			x				
Michael Homer		x	x		x	x	x	x		x				
Nigel Lee		x	x			x	x	x		x				
Ramon Ortiz						x	x	x		x				
Annalisa Patriarca						x	x			x				
Yolanda Prezado	x	x				x	x			x		x	x	x
Russell Thomas	x	x				x	x			x		x	x	x
Tony Price	x	x		x		x	x			x		x		x

References

[1] D.N. Slatkin, P. Spanne, F.A. Dilmanian and M. Sandborg, *Microbeam radiation therapy*, *Med. Phys.* **19** (1992) 1395.

[2] A. Bertho, R. Ortiz, M. Juchaux, C. Gilbert, C. Lamirault, F. Pouzoulet et al., *First evaluation of temporal and spatial fractionation in proton minibeam radiation therapy of glioma-bearing rats*, *Cancers* **13** (2021) 4865.

[3] Y. Prezado, *Proton minibeam radiation therapy: a promising therapeutic approach for radioresistant tumors*, *Comptes Rendus Biol.* **344** (2021) 409.

[4] C. Billena and A.J. Khan, *A current review of spatial fractionation: Back to the future?*, *Int. J. Radiat. Oncol. Biol. Phys.* **104** (2019) 177.

[5] W. Yan, M.K. Khan, X. Wu, C.B. Simone, J. Fan, E. Gressen et al., *Spatially fractionated radiation therapy: History, present and the future*, *Clin. Transl. Radiat. Oncol.* **20** (2020) 30.

[6] P. Cahoon, V. Giacometti, F. Casey, E. Russell, C. McGarry, K.M. Prise et al., *Investigating spatial fractionation and radiation induced bystander effects: a mathematical modelling approach*, *Phys. Med. Biol.* **66** (2021) 225007.

[7] A. Bertho, L. Iturri, E. Brisebard, M. Juchaux, C. Gilbert, R. Ortiz et al., *Evaluation of the role of the immune system response after minibeam radiation therapy*, *Int. J. Radiat. Oncol. Biol. Phys.* **115** (2023) 426.

[8] J. Archer, E. Li, J. Davis, M. Cameron, A. Rosenfeld and M. Lerch, *High spatial resolution scintillator dosimetry of synchrotron microbeams*, *Sci. Rep.* **9** (2019) 6873.

[9] J. Bartz, G. Sykora, E. Bräuer-Krisch and M. Akselrod, *Imaging and dosimetry of synchrotron microbeam with aluminum oxide fluorescent detectors*, *Radiat. Meas.* **46** (2011) 1936.

[10] J.A. Davis, E. Engels, M. Petasecca, J. Paino, M. Tehei, S. Corde et al., *X-TREAM protocol for in vitro microbeam radiation therapy at the australian synchrotron*, *J. Appl. Phys.* **129** (2021) 244902.

[11] Y. Prezado, I. Martínez-Rovira, S. Thengumpallil and P. Deman, *Dosimetry protocol for the preclinical trials in white-beam minibeam radiation therapy*, *Med. Phys.* **38** (2011) 5012.

[12] IBA Dosimetry, *myQA SRS*, https://www.iba-dosimetry.com/product/myqa-srs/.

[13] S. Bartzsch, J. Lott, K. Welsch, E. Bräuer-Krisch and U. Oelfke, *Micrometer-resolved film dosimetry using a microscope in microbeam radiation therapy*, *Med. Phys.* **42** (2015) 4069.

[14] E. Lee, J. Meyer and G. Sandison, *Collimator design for spatially-fractionated proton beams for radiobiology research*, *Phys. Med. Biol.* **61** (2016) 5378.

[15] E. Bräuer-Krisch, A. Bravin, L. Zhang, E. Siegbahn, J. Stepanek, H. Blattmann et al., *Characterization of a tungsten/gas multislit collimator for microbeam radiation therapy at the european synchrotron radiation facility*, *Rev. Sci. Instrum.* **76** (2005) 064303.

[16] Y. Prezado and G.R. Fois, *Proton-minibeam radiation therapy: A proof of concept*, *Med. Phys.* **40** (2013) 031712.

[17] Y. Prezado, M.D. Santos, W. Gonzalez, G. Jouvion, C. Guardiola, S. Heinrich et al., *Transfer of minibeam radiation therapy into a cost-effective equipment for radiobiological studies: a proof of concept*, *Sci. Rep.* **7** (2017) 17295.

2023 JINST 18 P03014

[18] Y. Prezado, G. Jouvion, D. Hardy, A. Patriarca, C. Nauraye, J. Bergs et al., *Proton minibeam radiation therapy spares normal rat brain: Long-term clinical, radiological and histopathological analysis*, *Sci. Rep.* **7** (2017) 14403.

[19] C. Lamirault, V. Doyère, M. Juchaux, F. Pouzoulet, D. Labiod, R. Dendale et al., *Short and long-term evaluation of the impact of proton minibeam radiation therapy on motor, emotional and cognitive functions*, *Sci. Rep.* **10** (2020) 13511.

[20] L.M. Petrie, *Characterisation of a Graphite Calorimeter in Scanned Proton Beams*, Ph.D. thesis, University of Surrey, U.K. (2016).

[21] S. Flynn, *Enhancement of the U.K. Primary Standard for Absorbed Dose for Proton Radiotherapy*, Ph.D. thesis, University of Birmingham, Birmingham, U.K. (2021).

[22] A. Lourenço, N. Lee, D. Shipley, F. Romano, A. Kacperek, S. Duane et al., *Application of a portable primary standard level graphite calorimeter for absolute dosimetry in a clinical low-energy passively scattered proton beam*, *Phys. Med. Biol.* **67** (2022) 225021.

[23] Nordson Test & Inspection, *Detectors*, https://www.nordson.com/en/divisions/test-inspection/nordson-x-ray-technologies/detectors.

[24] S. Flynn, S. Manolopoulos, V. Rompokos, A. Poynter, A. Toltz, L. Beck et al., *Monitoring pencil beam scanned proton radiotherapy using a large format CMOS detector*, *Nucl. Instrum. Meth. A* **1033** (2022) 166703.

[25] S. Flynn, T. Price, P.P. Allport, I.S. Patallo, R. Thomas, A. Subiel et al., *Evaluation of a pixelated large format CMOS sensor for x-ray microbeam radiotherapy*, *Med. Phys.* **47** (2020) 1305.

[26] S. Flynn, T. Price, P.P. Allport, I.S. Patallo, R. Thomas, A. Subiel et al., *First demonstration of real-time in-situ dosimetry of x-ray microbeams using a large format CMOS sensor*, *Nucl. Instrum. Meth. A* **978** (2020) 164395.

[27] A. Patriarca and S. Meyroneinc, *Proton therapy at the Institut Curie – CPO: Operation of an IBA C235 cyclotron looking forward scanning techniques*, in *Proceedings of the 20th International Conference on Cyclotrons and their Applications*, Vancouver, BC, Canada, 16–20 September 2013, pp. 403–405.

[28] C. Guardiola, C. Peucelle and Y. Prezado, *Optimization of the mechanical collimation for minibeam generation in proton minibeam radiation therapy*, *Med. Phys.* **44** (2017) 1470.

[29] A. Lourenço, N. Lee, D. Shipley, F. Romano, A. Kacperek, S. Duane et al., *Application of a portable primary standard level graphite calorimeter for absolute dosimetry in a clinical low-energy passively scattered proton beam*, *Phys. Med. Biol.* **67** (2022) 225021.

[30] S.R. Domen, *Calorimeter*, U.S. Patent US3665762A, 1972, https://patents.google.com/patent/US3665762A.

[31] PTW Freiburg GmbH, *Roos Electron Chamber*, https://www.ptwdosimetry.com/en/products/roos-electron-chamber/.

[32] Phoenix Dosimetry, *Bart's Solid Water for Electrons and Photons*, https://phoenix-dosimetry.co.uk/solid-water-and-bolus-material/.

[33] F.A. Bessia, M. Perez, M.S. Haro, I. Sidelnik, J.J. Blostein, S. Suarez et al., *Displacement damage in CMOS image sensors after thermal neutron irradiation*, *IEEE Trans. Nucl. Sci.* **65** (2018) 2793.

[34] International Atomic Energy Agency., *Accuracy requirements and uncertainties in radiotherapy*, International Atomic Energy Agency, Vienna (2016).

2023 JINST 18 P03014

[35] Ashland, *Gafchromic™ Dosimetry Media, Type EBT-3*, http://www.gafchromic.com/gafchromic-film/radiotherapy-films/EBT/index.asp.

[36] J. Winiecki, T. Morgaś, K. Majewska and B. Drzewiecka, *The gamma evaluation method as a routine QA procedure of IMRT*, *Rep. Pract. Oncol. Radiother.* **14** (2009) 162.

[37] R. Ortiz, L.D. Marzi and Y. Prezado, *Preclinical dosimetry in proton minibeam radiation therapy: Robustness analysis and guidelines*, *Med. Phys.* **49** (2022) 5551.

[38] M. Hussein, C. Clark and A. Nisbet, *Challenges in calculation of the gamma index in radiotherapy — towards good practice*, *Phys. Med.* **36** (2017) 1.

[39] C. Fernandez-Palomo, S. Chang and Y. Prezado, *Should peak dose be used to prescribe spatially fractionated radiation therapy?—a review of preclinical studies*, *Cancers* **14** (2022) 3625.

[40] *PyMedPhys*, https://pymedphys.com/.

[41] E. Bräuer-Krisch, J.-F. Adam, E. Alagoz, S. Bartzsch, J. Crosbie, C. DeWagter et al., *Medical physics aspects of the synchrotron radiation therapies: Microbeam radiation therapy (MRT) and synchrotron stereotactic radiotherapy (SSRT)*, *Phys. Med.* **31** (2015) 568.

[42] N. Annabell, N. Yagi, K. Umetani, C. Wong and M. Geso, *Evaluating the peak-to-valley dose ratio of synchrotron microbeams using PRESAGE fluorescence*, *J. Synchrotron Radiat.* **19** (2012) 332.

[43] Ashland, *Gafchromic™ Dosimetry Media, Type EBT-XD*, http://www.gafchromic.com/gafchromic-film/radiotherapy-films/EBT/index.asp.

[44] COMSOL Multiphysics, *About COMSOL*, https://uk.comsol.com/company.

[45] L. Allen, A. O'Connell and V. Kiermer, *How can we ensure visibility and diversity in research contributions? how the contributor role taxonomy (CRediT) is helping the shift from authorship to contributorship*, *Learn. Publ.* **32** (2019) 71.

2023 JINST 18 P03014